Chinese Journal of Chemical Engineering 70 (2024) 130–138

Contents lists available at ScienceDirect

Chinese Journal of Chemical Engineering

journal homepage: www.elsevier.com/locate/CJChE

Full Length Article

Synthesis of NaY zeolite from a submolten depolymerized perlite: Alkalinity effect and crystallization kinetics

Yanli Qu [1, 2], Peng Dong [3], Li Yang [1], Yuanyuan Yue [3, 4], Haoliang Wang [1], Jingcai Cheng [1, *], Chao Yang [1, 2]

[1] CAS Key Laboratory of Green Process and Engineering, State Key Laboratory of Petroleum Molecular & Process Engineering, Institute of Process Engineering, Chinese Academy of Sciences, Beijing 100190, China
[2] School of Chemical Engineering, University of Chinese Academy of Sciences, Beijing 100190, China
[3] Qingyuan Innovation Laboratory, Quanzhou 362801, China
[4] National Engineering Research Center of Chemical Fertilizer Catalyst, College of Chemical Engineering, Fuzhou University, Fuzhou 350108, China

ARTICLE INFO

Article history:
Received 21 January 2024
Received in revised form
14 March 2024
Accepted 14 March 2024
Available online 8 April 2024

Keywords:
NaY zeolite
Submolten salt depolymerized perlite
Alkalinity
Crystallization kinetics

ABSTRACT

NaY zeolites are synthesized using submolten salt depolymerized natural perlite mineral as the main silica and alumina sources in a 0.94 L stirred crystallizer. Effects of alkalinity ranging from 0.38 to 0.55 ($n(Na_2O)/n(SiO_2)$) on the relative crystallinity, textural properties and crystallization kinetics were investigated. The results show that alkalinity exerts a nonmonotonic influence on the relative crystallinity and textural properties, which exhibit a maximum at the alkalinity of 0.43. The nucleation kinetics are studied by fitting the experimental data of relative crystallinity with the Gualtieri model. It is shown that the nucleation rate constant increases with increasing alkalinity, while the duration period of nucleation decreases with increasing alkalinity. For $n(Na_2O)/n(SiO_2)$ ratios ranging from 0.38 to 0.55, the as-synthesized NaY zeolites exhibit narrower crystal size distributions with the increase in alkalinity. The growth rates determined from the variations of average crystal size with time are 51.09, 157.50, 46.17 and 24.75 $nm \cdot h^{-1}$, respectively. It is found that the larger average crystal sizes at the alkalinity of 0.38 and 0.43 are attributed to the dominant role of crystal growth over nucleation. Furthermore, the combined action of prominent crystal growth and the longer duration periods of nucleation at the alkalinity of 0.38 and 0.43 results in broader crystal size distributions. The findings demonstrate that control of the properties of NaY zeolite and the crystallization kinetics can be achieved by conducting the crystallization process in an appropriate range of alkalinity of the reaction mixture.

1. Introduction

Zeolites are crystalline aluminosilicate materials with unique pore structures, large specific surface area, tunable acidity and high thermal/hydrothermal stability. Because of these superior characteristics, zeolites have been widely used as catalysts, adsorbents and ion exchangers in the fields of oil refining, petrochemical and fine chemical industries [1–4]. The zeolite Y belongs to the faujasite framework and possesses three-dimensional 12-membered ring channels and spherical supercages. As one of the most important zeolites applied in catalysis, zeolite Y has shown remarkable activity, selectivity and hydrothermal stability in fluid catalytic cracking and hydrocracking reactions [5–7].

Synthesis of aluminosilicate zeolites typically involves the usage of aluminum- and silicon-containing chemical reagents as the raw materials. However, production processes of these chemicals are usually associated with huge energy consumption and waste generation. Thus, from green and economic perspectives, direct synthesis of zeolites from low-cost and environmentally friendly raw materials has been pursued. One such effort is utilizing natural aluminosilicate minerals with abundant reserves as alternative silica and alumina sources for synthesizing zeolites [8–11]. Most aluminosilicate minerals in their natural state have stable structure and are chemically inert. They cannot be utilized directly for synthesizing zeolites with high purity and crystallinity. Therefore, they need to be activated sufficiently into reactive silicon and aluminum species prior to

* Corresponding author.
E-mail address: jccheng@ipe.ac.cn (J. Cheng).

https://doi.org/10.1016/j.cjche.2024.03.009

the synthesis of zeolites. Commonly used activation methods include thermal activation, alkali fusion activation and acid leaching [11]. Li *et al.* [12] reported an effective activation method of natural aluminosilicates using submolten salt medium for the purpose of zeolite synthesis. It can be conducted at a lower temperature than that commonly used in the thermal activation process. And it has shown success in synthesizing various zeolites with desirable properties [13–16].

The control and optimization of the properties of a zeolite product necessitate a deep understanding of the nucleation and growth kinetics, such as the crystal size and crystal size distribution (CSD) which can greatly affect the catalytic performance [17–21]. Some experimental methods and mathematical models have been developed for the purpose of resolving the nucleation and crystal growth kinetics of zeolite crystallization. Li *et al.* [22–25] utilized a two-stage varying-temperature technique to investigate the crystallization kinetics of silicalite-1 and zeolite Y. The nucleation and crystal growth rates were determined from the temporal evolution of crystal concentration and average crystal size, respectively. This method is based on the fact that the nucleation process can be effectively halted when the temperature is abruptly increased. Thus the exact time period of the nucleation and growth processes can be resolved by varying the synthesis temperature at various time points during the course of a crystallization.

A commonly used modeling method for obtaining the kinetic parameters is by fitting the experimental crystallization curves with the Avrami-Erofe'ev equation [26–28] or the Gualtieri model [29]. Corregidor *et al.* [30] studied the influence of temperature on the crystallization kinetics of ZSM-5 zeolite with the Avrami-Erofe'ev equation. Nakhaei Pour and Mohammadi [31] studied the effects of Na_2O content in the initial gel and crystallization temperature on the crystallization kinetics of zeolite Y with the Avrami-Erofe'ev equation. Chen *et al.* [15] investigated the crystallization kinetics of zeolite NaA with the Avrami-Erofe'ev equation. Liu *et al.* [32] investigated the influence of the crystallization temperature on the nucleation and growth rates of zeolite T synthesized using zeolite seed solution with the Gualtieri model. Dewes *et al.* [33] studied the effect of ultrasound on the crystallization kinetics of zeolite A with the Gualtieri model. The dramatic advantage of the Gualtieri model over the Avrami-Erofe'ev equation is that it includes a probability function for nucleation which provides a qualitative estimate of variation of the nucleation rate with time and the extent of the temporal overlap between nucleation and crystal growth processes.

It has been reported that the alkalinity of the reaction mixture has great impact on the crystal size, morphology, nucleation and growth kinetics during the course of zeolite crystallization [34–36]. However, compared with other types of zeolite, the study of the effect of alkalinity on the crystallization kinetics of zeolite Y is still lacking, especially for those synthesized from natural aluminosilicate minerals. Thus in this contribution, NaY zeolites were synthesized from the submolten salt depolymerized natural perlite mineral in a 0.94 L stirred crystallizer. The effects of alkalinity ($n(Na_2O)/n(SiO_2)$) of the reaction mixture on the relative crystallinity, textural properties, average crystal size, CSD and crystallization kinetics were investigated in detail.

2. Experimental

2.1. Materials

The natural perlite mineral was purchased from Xinyang Pingqiao District Sitong Thermal Insulation Material Co., Ltd. (Henan province, China). And its chemical composition is listed in Table 1. Sodium hydroxide (≥98% (mass)) and sodium aluminate (46.78% (mass) Na_2O and 53.08% (mass) Al_2O_3) were purchased from Shanghai Macklin Biochemical Co., Ltd. (China). Sulfuric acid (98% (mass)) was supplied by Sinopharm Chemical Reagent Co., Ltd. (Shanghai, China). Silica sol (30% (mass) SiO_2) was purchased from Beijing Hongxing Chemical Building Materials Co., Ltd. (China). The commercial NaY zeolite used as the reference was acquired from Nankai University Catalyst Co., Ltd. (Tianjin, China). All the materials were used as received without any further purification.

Table 1
Chemical composition of the natural perlite mineral

Component	SiO_2	Al_2O_3	K_2O	Na_2O	CaO	Fe_2O_3	MgO	TiO_2
Content/% (mass)	76.08	13.74	5.36	2.27	1.11	0.83	0.28	0.11

2.2. Depolymerization of the natural perlite mineral

The natural perlite mineral was depolymerized in a submolten salt (SMS) medium as described elsewhere [12]. Typically, 120 g of sodium hydroxide was added into a 2 L open Teflon beaker containing 600 g of deionized water under agitation. Then 100 g of the natural perlite was appended to the sodium hydroxide solution. Finally, the suspension was placed into an oven exposed to air at 300 °C for 2 h.

2.3. Preparation of the inorganic structure-directing agent

The inorganic structure-directing agent (SDA) with a molar composition of 15.6 Na_2O:1 Al_2O_3:15 SiO_2:294 H_2O was prepared as follows. 17.29 g of sodium aluminate and 102.64 g of sodium hydroxide were added into a 1 L beaker containing 288.37 g of deionized water. The system was stirred until a complete dissolution of the solids. Then 269.76 g of silica sol was added slowly under vigorous stirring. After being further stirred for 1.5 h, the mixture was aged at room temperature for 24 h.

2.4. Synthesis of NaY zeolite

NaY zeolites were synthesized with molar compositions of x Na_2O:1 Al_2O_3:12.5 SiO_2:375 H_2O, where x = 4.750, 5.375, 6.250 and 6.875. In a typical synthesis experiment, 85.00 g of SMS depolymerized perlite was mixed with an appropriate amount of deionized water and the suspension was stirred for 5 min. Then 29.50 g of silica sol and 43.58 g of SDA were added into the suspension under stirring. Next for $n(Na_2O)/n(SiO_2)$ ratios ranging from 0.38 to 0.55, appropriate amounts of 50% (mass) sulfuric acid were added to adjust the pH values of the synthesis system to 12.75, 12.95, 13.18 and 13.32, respectively. After being stirred further for 5 min, the reactant mixture was transferred into a 0.94 L stainless-steel crystallizer equipped with a 45° upward impeller as shown in Fig. 1. The mixture was aged at 40 °C for 6 h with a stirring rate of 600 $r \cdot min^{-1}$ and crystallized at 95 °C for different times with a stirring rate of 400 $r \cdot min^{-1}$. After termination of the crystallization, the solid and liquid fractions of samples were separated by filtration. The solid product was washed thoroughly with deionized water until the pH value of the filtrate was close to neutral and then was dried overnight at 105 °C.

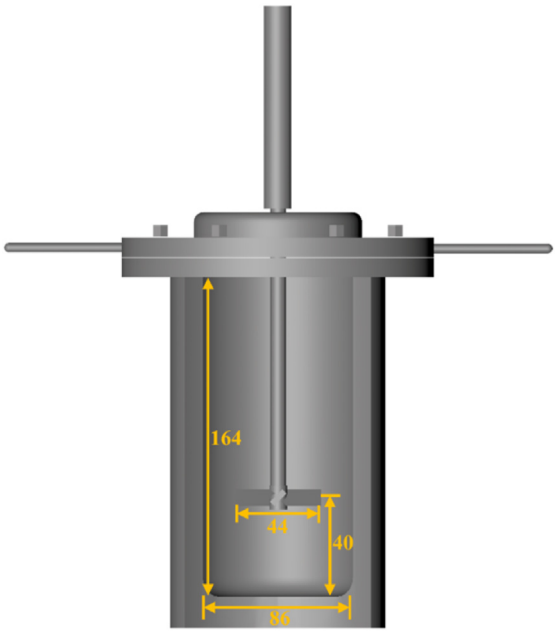

Fig. 1. Configuration of the crystallizer for synthesis of NaY zeolite (unit: mm).

2.5. Characterizations

The powder X-ray diffraction patterns were collected on a Rigaku Smartlab diffractometer (Japan) with Cu K_α radiation operated at 45 kV and 200 mA. The scanning 2θ range was 5°–40° with a step size of 0.01° and a scan speed of 4 (°)·min^{-1}. The relative crystallinity of the solid product was calculated by comparison of the sum of the diffraction peak areas at reflections of the (*h k l*) values of (3 1 1), (3 3 3), (4 4 0), (5 3 3), (6 4 2), (6 6 0), (5 5 5) and (6 6 4) with those of the commercial NaY zeolite, whose crystallinity was considered to be 100%. The unit cell parameters (a_0) of the as-synthesized NaY samples and the commercial NaY zeolite were determined using pure silicon (99.999% (mass)) as the internal standard for angle calibration ($2\theta = 28.443°$) according to SH/T 0339—92. The scanning range was 28°–32° with a scan speed of 0.2(°)·min^{-1}. The framework SiO_2/Al_2O_3 ratios (SAR) were calculated by Eq. (1) [37].

$$\mathrm{SAR} = \frac{2 \times (25.858 - a_0)}{a_0 - 24.191} \tag{1}$$

Scanning electron microscopy (SEM) observation was performed on a Zeiss GeminiSEM 300 (UK) instrument at an accelerating voltage

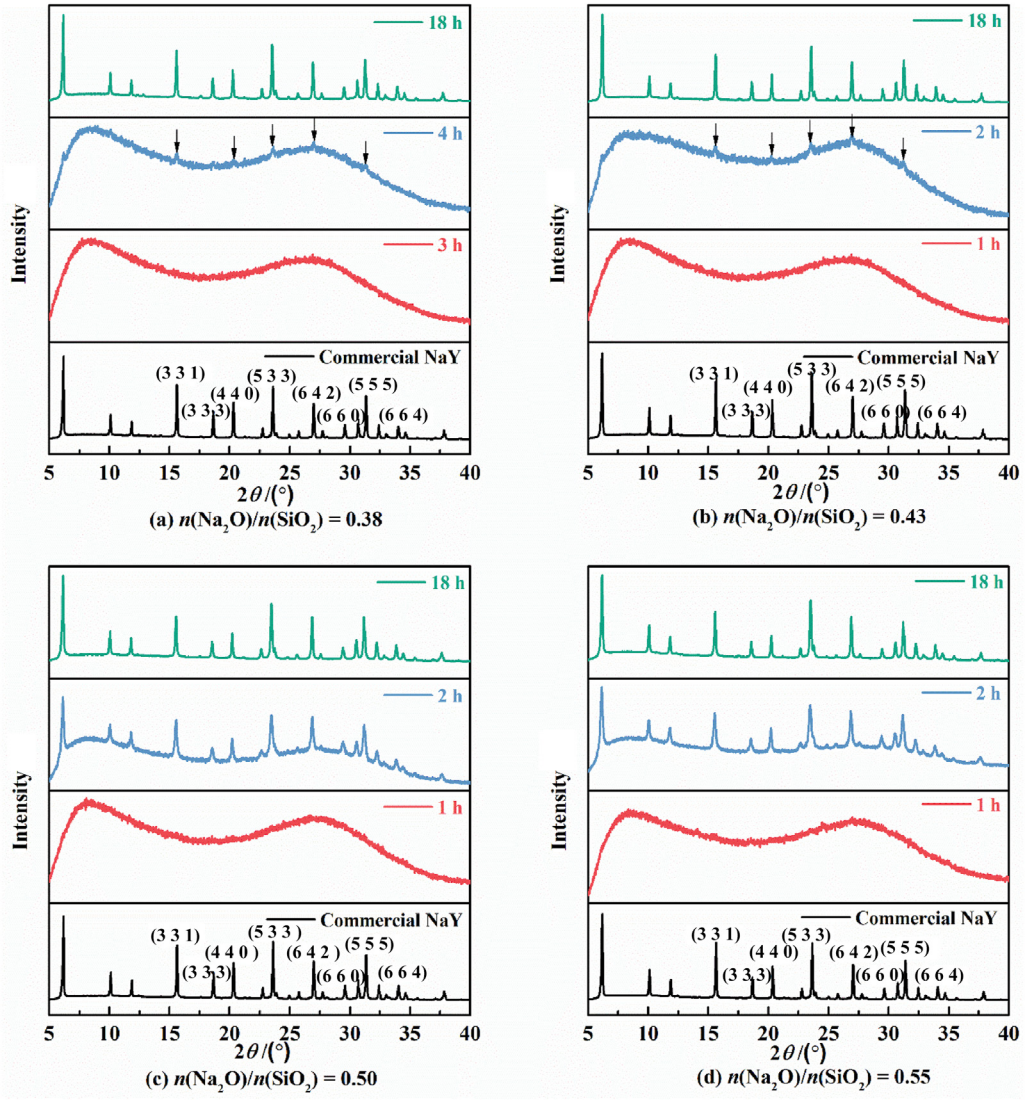

Fig. 2. XRD patterns of solid products obtained at different crystallization times under various $n(Na_2O)/n(SiO_2)$ ratios.

of 2 kV. More than 200 NaY zeolite particles were analyzed to extract the average crystal size and CSD from the SEM images.

The chemical composition of the natural perlite mineral was analyzed by X-ray fluorescence (XRF) conducted on a PANalytical B.V. AXIOS instrument (Netherlands).

N_2 adsorption–desorption measurements were performed on a Quantachrome Autosorb-iQ (USA) instrument at −196 °C. The solid samples were degassed and dehydrated in vacuum at 300 °C for 8 h prior to measurement. The specific surface areas (S_{BET}) were calculated by the Brunauer-Emmett-Teller (BET) method in the P/P_0 range of 0.0002–0.02. The pore volumes (V_{total}) are obtained at P/P_0 = 0.99. The micropore specific surface areas (S_{micro}), external specific areas (S_{ext}) and micropore volumes (V_{micro}) were determined by the *t*-plot method.

3. Results and Discussion

3.1. Characteristics of as-synthesized NaY zeolites

3.1.1. Effect of n(Na_2O)/n(SiO_2) ratio on relative crystallinity

The representative XRD patterns of the solid products obtained at different crystallization times under various $n(Na_2O)/n(SiO_2)$ ratios are shown in Fig. 2. At a crystallization time of 18 h, the XRD patterns of all the solid products present characteristic peaks of the FAU-type zeolite, indicating the successful synthesis of pure-phase NaY zeolites. However, the alkalinity of the synthesis system shows a noticeable effect on the induction period of the crystallization process. With the increase in $n(Na_2O)/n(SiO_2)$ ratio, the induction period is shortened from 3 h to 1 h. Furthermore, the difference in the intensity of the characteristic peaks at a crystallization time of 2 h suggests that in spite of being of the same induction period, the amount of the NaY zeolite phase in the solid product is higher for alkalinities of 0.50 and 0.55 than that of 0.43.

The qualitative information displayed by the XRD patterns is quantified by the relative crystallinity of the solid product as shown in Fig. 3, which presents the variation of relative crystallinity with crystallization time under different $n(Na_2O)/n(SiO_2)$ ratios. It can be seen that for crystallization times shorter than 6 h, a higher alkalinity leads to a higher relative crystallinity of NaY zeolite. With the increase in alkalinity, the time needed to attain a final equilibrium is shortened from 12 h to 8 h and further to 6 h. The equilibrium relative crystallinity first increases from 64% to 71% and then decreases to 58%.

From the crystallization curves as shown in Fig. 3, it can be concluded that the alkalinity of the synthesis system affects both the crystallization rate and the relative crystallinity at equilibrium. For the investigated range of $n(Na_2O)/n(SiO_2)$ ratio in this work, a tradeoff between the crystallization rate and the equilibrium value of relative crystallinity makes 0.43 the optimal alkalinity condition for the synthesis system.

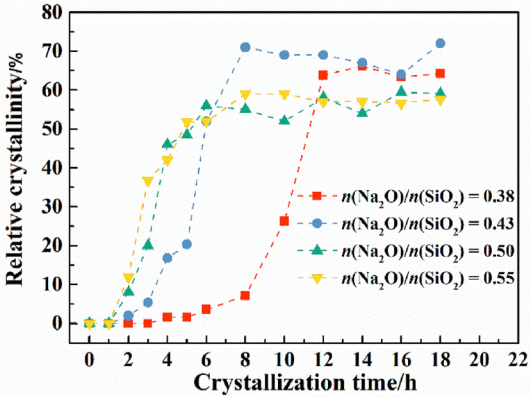

Fig. 3. Relative crystallinity of the solid products obtained at different crystallization times under various $n(Na_2O)/n(SiO_2)$ ratios.

The framework SARs of the commercial NaY zeolite and as-synthesized NaY zeolite samples at a crystallization time of 18 h under various alkalinity conditions are displayed in Fig. 4. It shows that increasing the alkalinity of the reaction system results in a low framework SAR, as reported by Delprato *et al.* [38]. The increase in alkalinity leads to more dissolution of silica, thus resulting in a decreased framework SAR.

3.1.2. Effect of n(Na_2O)/n(SiO_2) ratio on textural properties

The results of N_2 adsorption-desorption are shown in Fig. 5. All the solid products crystallized for 18 h exhibit type I isotherms, indicating that the as-synthesized NaY zeolites are all typical microporous materials [39,40]. The textural parameters of the as-synthesized NaY zeolites at a crystallization time of 18 h and the commercial NaY zeolite are listed in Table 2.

As can be expected from the results of relative crystallinity, the S_{micro} and V_{micro} of the as-synthesized NaY zeolites are lower than those of the commercial NaY zeolite. And the solid product synthesized at the alkalinity of 0.43 possesses the highest S_{micro} and V_{micro}, which are 545 $m^2 \cdot g^{-1}$ and 0.21 $cm^3 \cdot g^{-1}$, respectively. Compared with the NaY zeolite synthesized at the alkalinity of 0.38, the solid products synthesized at the alkalinity of 0.50 and 0.55 show a 54% and 85% increment in the mesopore volume, respectively. Considering the microporous characteristics of the as-synthesized NaY zeolites, these mesopores are produced from the smaller inter-crystalline agglomerates.

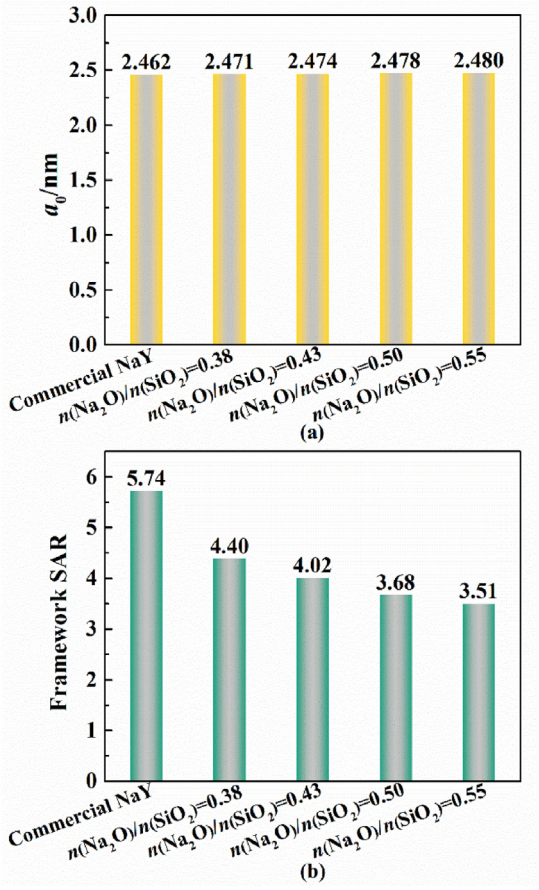

Fig. 4. (a) Unit cell parameters and (b) framework SARs of the commercial NaY zeolite and as-synthesized NaY zeolite samples at a crystallization time of 18 h under various alkalinity conditions.

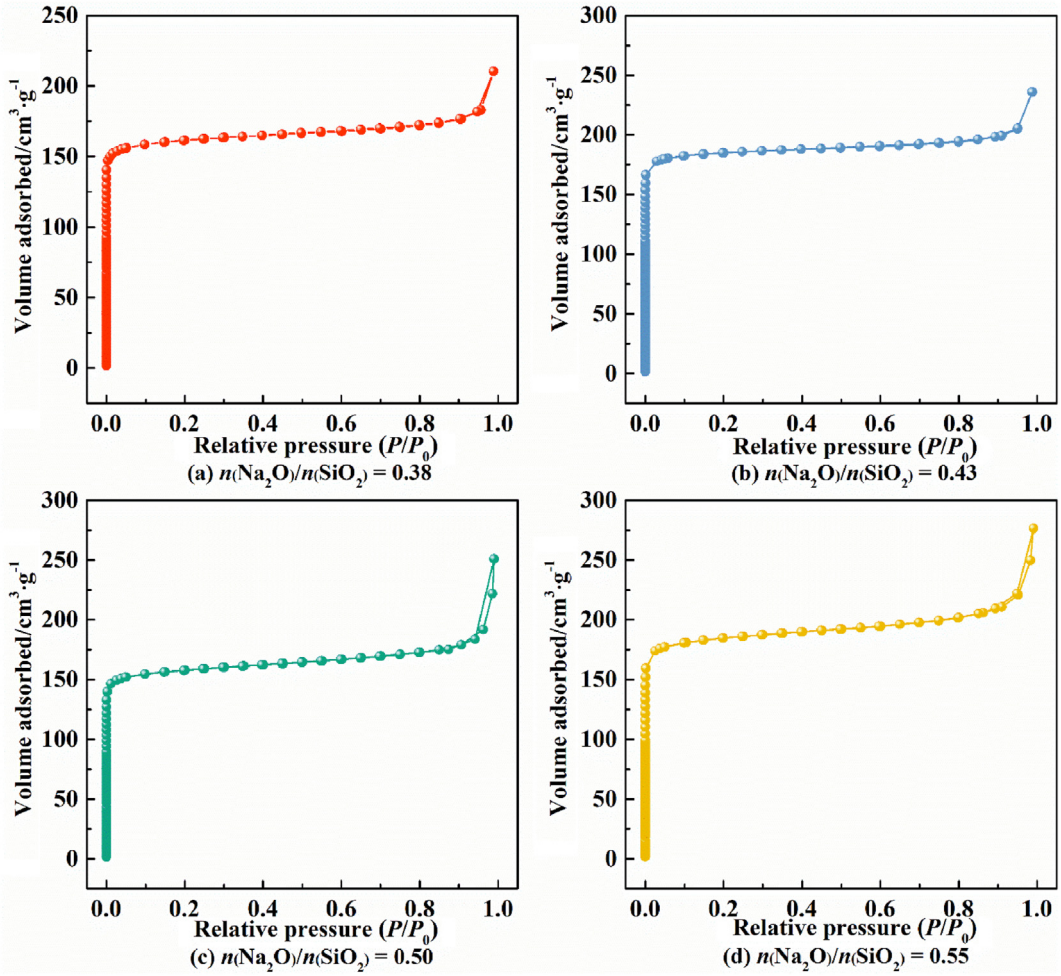

Fig. 5. N_2 adsorption–desorption isotherms of as-synthesized NaY zeolites obtained at a crystallization time of 18 h under various $n(Na_2O)/n(SiO_2)$ ratios.

3.2. Crystallization kinetics study

3.2.1. Nucleation kinetics

Nucleation kinetics of the crystallization process was investigated by the model introduced by Gualtieri [29]. The Gualtieri model describes the evolution of the relative crystallinity with time by

$$\alpha = \frac{1-\exp\left[-(k_g t)^n\right]}{1+\exp\left(-\frac{t-a}{b}\right)} \tag{2}$$

where α is the relative crystallinity, k_g is the growth rate constant, and a and b are two parameters related to the nucleation. In the Gualtieri model, the nucleation kinetics is estimated by defining a probability of nucleation P_N with a Gaussian distribution.

$$P_N = \exp\left[-\frac{(t-a)^2}{2b^2}\right] \tag{3}$$

In Eq. (3), the parameter a is the time at which the nucleation attains the maximum rate. The parameter b is the variance of the probability curve and its value can give insight into the nucleation mechanism.

The four model parameters in Eq. (2) are estimated by minimizing the sum of squared errors between the experimental data of relative crystallinity and the Gualtieri model predictions. The objective function is represented by the following equation

Table 2
Textural parameters of the commercial NaY zeolite and the as-synthesized NaY zeolites obtained at a crystallization time of 18 h under various $n(Na_2O)/n(SiO_2)$ ratios

$n(Na_2O)/n(SiO_2)$	S_{BET}/m^2·g^{-1}	S_{micro}/m^2·g^{-1}	S_{ext}/m^2·g^{-1}	V_{total}/cm^3·g^{-1}	V_{micro}/cm^3·g^{-1}	V_{meso}[①]/cm^3·g^{-1}
Commercial NaY	847	712	135	0.36	0.27	0.09
0.38	652	519	133	0.33	0.20	0.13
0.43	752	545	208	0.36	0.21	0.15
0.50	635	487	148	0.39	0.19	0.20
0.55	740	459	281	0.43	0.19	0.24

① $V_{meso} = V_{total} - V_{micro}$.

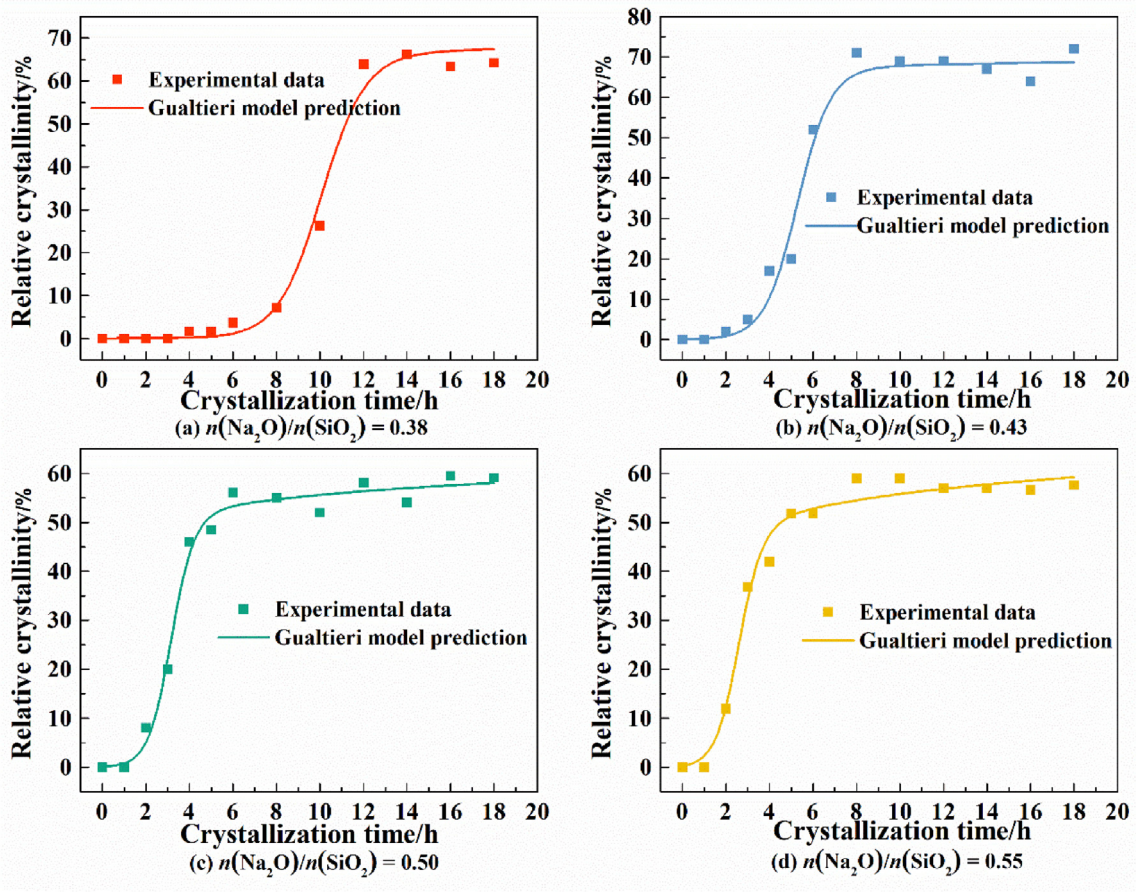

Fig. 6. Crystallization curves fitted by the Gualtieri model under various $n(Na_2O)/n(SiO_2)$ ratios.

$$\min_{\theta}\left\{\varepsilon=\sum_{i}^{N_t}\left[\alpha_{\exp}(t_i)-\alpha_{\text{model}}(t_i;\theta)\right]^2\right\} \tag{4}$$

where $\theta=[a, b, n, k_g]$ is the vector of fitted model parameters, N_t is the number of discrete time points, $\alpha_{\exp}(t_i)$ and $\alpha_{\text{model}}(t_i;\theta)$ are the experimental values and model predictions at time t_i, respectively. Eq. (4) is solved using an unstrained optimization algorithm based on a derivative-free simplex search algorithm (fminsearch function in MATLAB R2019a). Comparisons between the experimental data and model prediction are shown in Fig. 6. And the values of model parameters and fitting results are given in Table 3.

The parameter k_n in Table 3 is the nucleation rate constant defined by

$$k_n=\frac{1}{a} \tag{5}$$

With the increase in alkalinity, the nucleation rate constant shows a significant increase from 0.0994 h^{-1} to 0.3924 h^{-1}. It demonstrates that the nucleation proceeds with a higher rate at higher alkalinity. Substituting the values of a and b in Table 3 into Eq. (3), the probability curves of nucleation P_N are plotted in Fig. 7. It is shown that a higher alkalinity leads to a shorter duration period of nucleation, which is also manifested by the decreasing value of parameter b with increasing alkalinity in Table 3. Furthermore, considerable overlaps between the nucleation probability curves with the increase in alkalinity suggest that there exists an appropriate range of alkalinity where a better control of the nucleation rate and its duration period can be achieved by adjusting the alkalinity of the synthesis system.

Table 3
Values of Gualtieri model parameters and fitting results at various $n(Na_2O)/n(SiO_2)$ ratios

$n(Na_2O)/n(SiO_2)$	a/h	b/h	n	k_g/h^{-1}	k_n/h^{-1}	ε
0.38	10.0558	1.0055	0.0598	0.3755	0.0994	0.0100
0.43	5.2776	0.7600	0.0363	3.4287	0.1895	0.0171
0.50	3.1329	0.5823	0.1140	0.0160	0.3192	0.0065
0.55	2.5484	0.5434	0.1583	0.0277	0.3924	0.0079

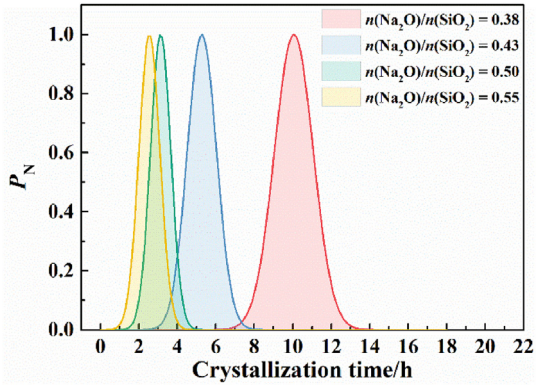

Fig. 7. Nucleation probability curves under various $n(Na_2O)/n(SiO_2)$ ratios.

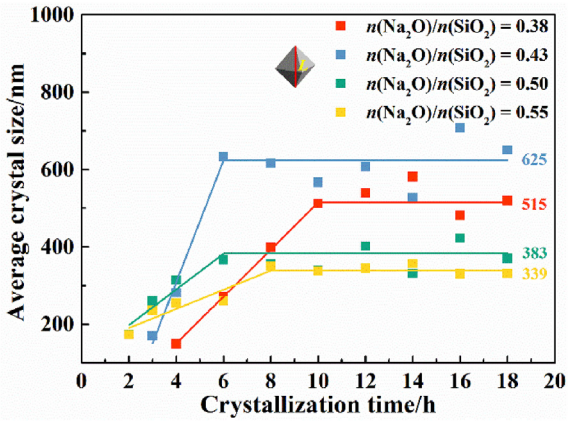

Fig. 8. Evolution of the average crystal size with crystallization time under various $n(Na_2O)/n(SiO_2)$ ratios.

3.2.2. Growth kinetics

The growth kinetics is studied by measuring the variation of average crystal size with crystallization time. The average crystal size of NaY zeolite is acquired from SEM images and is calculated by

$$\bar{L} = \frac{\sum_i N_i L_i}{\sum_i N_i} \tag{6}$$

where N_i is the number of crystals having a size between L and $L + \Delta L$ and $L_i = L + \Delta L/2$. The distance between two vertices of an octahedron is selected as the characteristic crystal size of a NaY zeolite.

Temporal evolutions of average crystal size under various $n(Na_2O)/n(SiO_2)$ ratios are shown in Fig. 8. It shows that the crystal population increases in size almost linearly during the crystallization process until reaching an equilibrium size. However, it is obvious that the increasing rate of average crystal size and its equilibrium size are distinct under various alkalinity conditions. For $n(Na_2O)/n(SiO_2)$ ratio ranging from 0.38 to 0.55, the growth rates quantified from the slopes of the curves are 51.09, 157.50, 46.17 and 24.75 $nm \cdot h^{-1}$, respectively. The final average crystal sizes are *ca.* 515, 625, 383 and 339 nm, respectively. It demonstrates the above discussion that the increases in S_{ext} result from their smaller crystal sizes at the alkalinity of 0.50 and 0.55.

The variations of CSD with time during the crystallization stage prior to equilibrium under various alkalinity conditions are shown in Fig. 9. It can be seen that with the increase in time, the crystal population moves along the positive direction of the crystal size axis, indicating the increase in the average crystal size. The crystal population exhibits the largest crystal size of *ca.* 700, 900 and 550 nm, respectively. Meanwhile, the span of the CSD becomes broader during the evolution process, which is more evident for CSDs at the alkalinity of 0.38 and 0.43 than those at the alkalinity of 0.50 and 0.55.

The final CSDs under different alkalinity conditions are shown in Fig. 10. It can be seen that the span of the CSD becomes narrower with the increase in alkalinity. It is known that the average crystal size and CSD result from the combined effect of nucleation and growth. In order to analyze the results of average crystal size and CSD from the perspective of crystallization kinetics, the ratios of

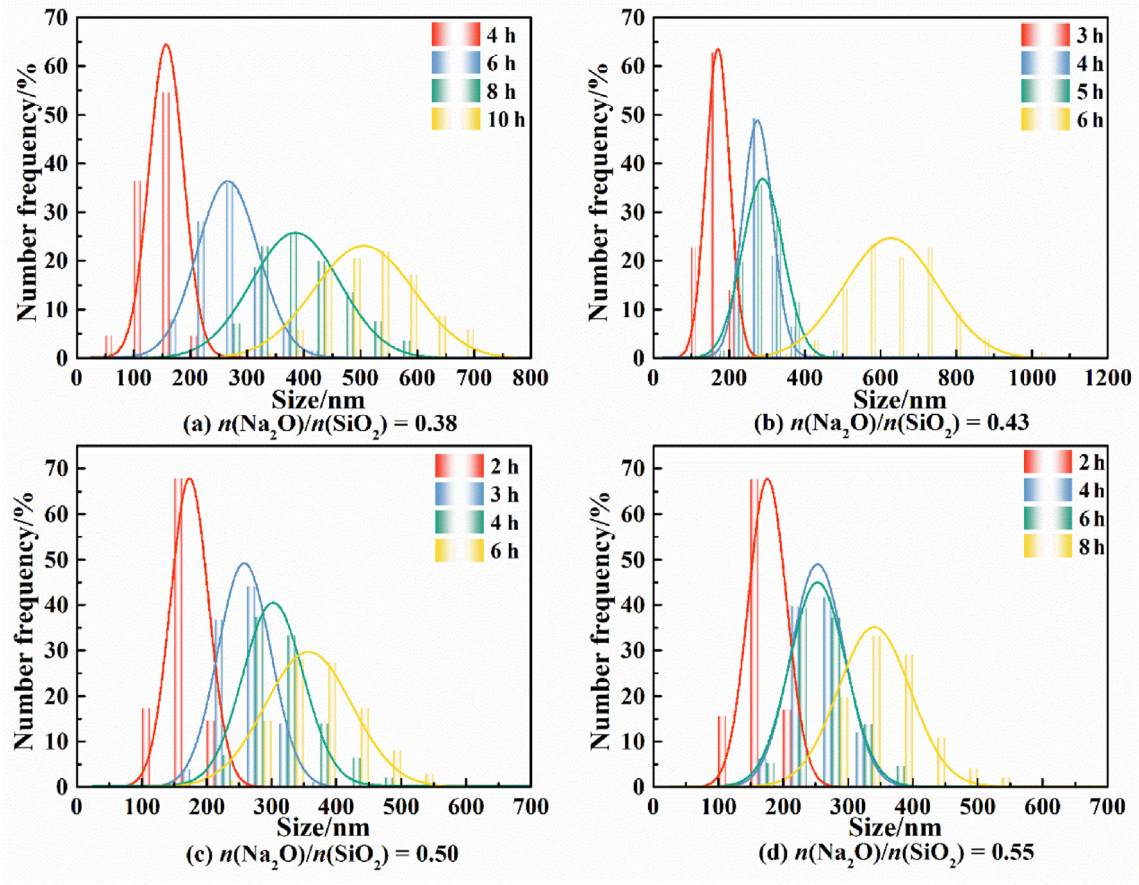

Fig. 9. Temporal evolution of CSDs under various $n(Na_2O)/n(SiO_2)$ ratios during the crystallization stage prior to equilibrium.

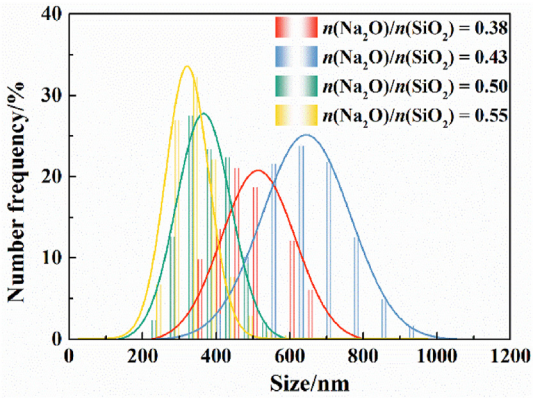

Fig. 10. Final CSDs of as-synthesized NaY zeolites under various $n(Na_2O)/n(SiO_2)$ ratios.

growth rate to nucleation rate constant under various alkalinity conditions are calculated to be 514, 832, 145 and 63, respectively. The higher ratios at the alkalinity of 0.38 and 0.43 indicate a dominant role of crystal growth over nucleation during the crystallization process, thus leading to larger final average crystal sizes. In addition, the combined action of prominent crystal growth and the longer duration periods of nucleation at the alkalinity of 0.38 and 0.43 results in broader CSDs.

4. Conclusions

In summary, NaY zeolites have been synthesized from a submolten salt depolymerized natural perlite mineral in a 0.94 L stirred crystallizer. The effects of alkalinity ranging from 0.38 to 0.55 on the relative crystallinity, textural properties, average crystal size, CSD and crystallization kinetics are studied in detail. The results show that the as-synthesized NaY zeolites exhibit the highest relative crystallinity and optimal textural properties at the alkalinity of 0.43. Crystallization kinetics studies show that in the investigated range of alkalinity, the nucleation rate constant increases with increasing alkalinity, while the duration period of nucleation decreases with increasing alkalinity. For $n(Na_2O)/n(SiO_2)$ ratios ranging from 0.38 to 0.55, the final average crystal sizes are *ca.* 515, 625, 383 and 339 nm, respectively. And the growth rates are determined to be 51.09, 157.50, 46.17 and 24.75 $nm \cdot h^{-1}$, respectively. The ratios of growth rate to nucleation rate constant suggest that at the alkalinity of 0.38 and 0.43, the larger average crystal sizes are attributed to the dominant role of crystal growth over nucleation. The broader CSDs at the alkalinity of 0.38 and 0.43 result from the combined action of prominent crystal growth and the longer duration periods of nucleation. The results in this work illustrate that control of the properties of NaY zeolite and the crystallization kinetics can be achieved by conducting the crystallization process in an appropriate range of alkalinity of the reaction mixture.

Declaration of Interest

The authors declare that they have no known competing financial interests or personal relationships that could have appeared to influence the work reported in this paper.

Acknowledgements

Financial supports from National Natural Science Foundation of China (21938009, 22308358, 22208346, 22078332), National Key Research and Development Program (2022YFC3902701), Ningxia Natural Science Foundation (2021AAC01002), the External Cooperation Program of BIC, Chinese Academy of Sciences (122111KYSB20190032) and CAS Project for Young Scientists in Basic Research (YSBR-038) are gratefully acknowledged.

Nomenclature

a	Gualtieri model parameter, h
a_0	unit cell parameter, nm
b	Gualtieri model parameter, h
k_g	Gualtieri model parameter, h^{-1}
k_n	nucleation rate constant, h^{-1}
$\bar{L}$	average crystal size, nm
N_t	number of discrete time points
n	Gualtieri model parameer
P_N	nucleation probability
S_{BET}	specific surface area, $m^2 \cdot g^{-1}$
S_{ext}	external specific surface area, $m^2 \cdot g^{-1}$
S_{micro}	micropore specific surface area, $m^2 \cdot g^{-1}$
t_i	time, h
V_{meso}	mesopore volume, $cm^3 \cdot g^{-1}$
V_{micro}	micropore volume, $cm^3 \cdot g^{-1}$
V_{total}	total pore volume, $cm^3 \cdot g^{-1}$
α	relative crystallinity
ε	sum of squared residuals
$\boldsymbol{\theta}$	model parameter vector

References

[1] Z.P. Wang, J.H. Yu, R.R. Xu, Needs and trends in rational synthesis of zeolitic materials, *Chem. Soc. Rev.* 41 (5) (2012) 1729–1741.
[2] Y. Li, J.H. Yu, New stories of zeolite structures: their descriptions, determinations, predictions, and evaluations, *Chem. Rev.* 114 (14) (2014) 7268–7316.
[3] C.G. Li, M. Moliner, A. Corma, Building zeolites from precrystallized units: Nanoscale architecture, *Angew. Chem. Int. Ed. Engl.* 57 (47) (2018) 15330–15353.
[4] X.Y. Li, H. Han, N. Evangelou, N.J. Wichrowski, P. Lu, W.Q. Xu, S.J. Hwang, W.Y. Zhao, C.S. Song, X.W. Guo, A. Bhan, I.G. Kevrekidis, M. Tsapatsis, Machine learning-assisted crystal engineering of a zeolite, *Nat. Commun.* 14 (1) (2023) 3152.
[5] D. Verboekend, N. Nuttens, R. Locus, J. Van Aelst, P. Verolme, J.C. Groen, J. Pérez-Ramírez, B.F. Sels, Synthesis, characterisation, and catalytic evaluation of hierarchical faujasite zeolites: Milestones, challenges, and future directions, *Chem. Soc. Rev.* 45 (12) (2016) 3331–3352.
[6] B. Meng, S.Y. Ren, X.Y. Liu, L. Zhang, Q.X. Hu, J.J. Wang, Q.X. Guo, B.J. Shen, Synthesis of USY zeolite with a high mesoporous content by introducing Sn and enhanced catalytic performance, *Ind. Eng. Chem. Res.* 59 (13) (2020) 5712–5719.
[7] D.L. Zhu, L.Y. Wang, W.N. Zhang, D. Fan, J.Z. Li, W.H. Cui, S.J. Huang, S.T. Xu, P. Tian, Z.M. Liu, Realizing fast synthesis of high-silica zeolite Y with remarkable catalytic performance, *Angew. Chem. Int. Ed. Engl.* 61 (23) (2022) e202117698.
[8] G. Garcia, E. Cardenas, S. Cabrera, J. Hedlund, J. Mouzon, Synthesis of zeolite Y from diatomite as silica source, *Microporous Mesoporous Mat.* 219 (2016) 29–37.
[9] J.Q. Wang, Y.X. Huang, Y.M. Pan, J.X. Mi, New hydrothermal route for the synthesis of high purity nanoparticles of zeolite Y from Kaolin and quartz, *Microporous Mesoporous Mat.* 232 (2016) 77–85.
[10] W.N. Wang, S.S. Kong, X.X. Zhou, D.L. Yuan, H. Li, S.Y. Ren, B.J. Shen, Perlite templated Y zeolite assembly and its potential as an efficient catalytic cracking catalyst, *Microporous Mesoporous Mat.* 243 (2017) 130–134.
[11] M. Feng, Z.R. Kou, C.Y. Tang, Z.M. Shi, Y.C. Tong, K.W. Zhang, Recent progress in synthesis of zeolite from natural clay, *Appl. Clay Sci.* 243 (2023) 107087.
[12] T.S. Li, H.Y. Liu, Y. Fan, P. Yuan, G. Shi, X.T. Bi, X.J. Bao, Synthesis of zeolite Y from natural aluminosilicate minerals for fluid catalytic cracking application, *Green Chem.* 14 (12) (2012) 3255.
[13] J.B. Yang, T.S. Li, X.J. Bao, Y.Y. Yue, H.Y. Liu, Mesoporogen-free synthesis of hierarchical sodalite as a solid base catalyst from sub-molten salt-activated aluminosilicate, *Particuology* 48 (2020) 48–54.
[14] Y.Y. Yue, X.X. Guo, T. Liu, H.Y. Liu, T.H. Wang, P. Yuan, H.B. Zhu, Z.S. Bai, X.J. Bao, Template free synthesis of hierarchical porous zeolite Beta with natural Kaolin clay as alumina source, *Microporous Mesoporous Mat.* 293 (2020) 109772.
[15] X.L. Chen, Y. Wang, C. Wang, J.D. Xu, T.S. Li, Y.Y. Yue, X.T. Bi, L.L. Jiang, X.J. Bao, Synthesis of NaA zeolite *via* the mesoscale reorganization of submolten salt depolymerized Kaolin: A mechanistic study, *Chem. Eng. J.* 454 (2023) 140243.

[16] P. Dong, J.Y. Zhang, T.S. Li, C. Wang, J.D. Xu, T.H. Wang, Y.Y. Yue, L.L. Jiang, X.J. Bao, Dealumination of Y zeolite through an economic and eco-friendly defect-engineering strategy, *AIChE. J.* 69 (9) (2023) e18183.
[17] M. Choi, K. Na, J. Kim, Y. Sakamoto, O. Terasaki, R. Ryoo, Stable single-unit-cell nanosheets of zeolite MFI as active and long-lived catalysts, *Nature* 461 (7261) (2009) 246–249.
[18] Q. Cui, Y. Zhou, Q. Wei, X. Tao, G. Yu, Y. Wang, J. Yang, Role of the zeolite crystallite size on hydrocracking of vacuum gas oil over NiW/Y-ASA catalysts, *Energy Fuel.* 26 (2012) 4664–4670.
[19] S. Hu, J. Shan, Q. Zhang, Y. Wang, Y.S. Liu, Y.J. Gong, Z.J. Wu, T. Dou, Selective formation of propylene from methanol over high-silica nanosheets of MFI zeolite, *Appl. Catal. A-Gen.* 445-446 (2012) 215–220.
[20] D. Karami, S. Rohani, The effect of particle-size reduction of zeolite Y on catalytic cracking of bulky hydrocarbons, *Pet. Sci. Technol.* 31 (16) (2013) 1625–1632.
[21] X.J. Dai, Y. Cheng, T.T. Liu, L.J. Mao, R.H. Kang, Q. Wei, Y.S. Zhou, Synthesis of small-crystal Y zeolites *via* regulating Na_2O/Al_2O_3 and superior catalytic performance of corresponding NiWS-supported catalysts for hydrocracking of naphthalene, *New J. Chem.* 47 (43) (2023) 20157–20170.
[22] Q. Li, D. Creaser, J. Sterte, The nucleation period for TPA-silicalite-1 crystallization determined by a two-stage varying-temperature synthesis, *Microporous Mesoporous Mat.* 31 (1–2) (1999) 141–150.
[23] Q.H. Li, B. Mihailova, D. Creaser, J. Sterte, The nucleation period for crystallization of colloidal TPA-silicalite-1 with varying silica source, *Microporous Mesoporous Mat.* 40 (1–3) (2000) 53–62.
[24] Q.H. Li, B. Mihailova, D. Creaser, J. Sterte, Aging effects on the nucleation and crystallization kinetics of colloidal TPA-silicalite-1, *Microporous Mesoporous Mat.* 43 (1) (2001) 51–59.
[25] Q.H. Li, D. Creaser, J. Sterte, An investigation of the nucleation/crystallization kinetics of nanosized colloidal faujasite zeolites, *Chem. Mat.* 14 (3) (2002) 1319–1324.
[26] M. Avrami, Kinetics of phase change. I General theory, *J. Chem. Phys.* 7 (1939) 1103–1112.
[27] M. Avrami, Kinetics of phase change. II Transformation-time relations for random distribution of nuclei, *J. Chem. Phys.* 8 (1940) 212–224.
[28] M. Avrami, Granulation, phase change, and microstructure kinetics of phase change. III, *J. Chem. Phys.* 9 (1941) 177–184.
[29] A.F. Gualtieri, Synthesis of sodium zeolites from a natural halloysite, *Phys. Chem. Miner.* 28 (10) (2001) 719–728.
[30] P.F. Corregidor, D.E. Acosta, H.A. Destéfanis, Kinetic study of seed-assisted crystallization of ZSM-5 zeolite in an OSDA-free system using a natural aluminosilicate as starting source, *Ind. Eng. Chem. Res.* 57 (41) (2018) 13713–13720.
[31] A. Nakhaei Pour, A. Mohammadi, Effects of synthesis parameters on organic template-free preparation of zeolite Y, *J. Inorg. Organomet. Polym. Mater.* 31 (6) (2021) 2501–2510.
[32] J. Liu, J.Y. Zhang, H.Z. Zhang, F. Zhang, M.H. Zhu, N. Hu, X.S. Chen, H. Kita, Synthesis of hierarchical zeolite T nanocrystals with the assistance of zeolite seed solution, *J. Solid State Chem.* 285 (2020) 121228.
[33] R.M. Dewes, H.R. Mendoza, M.V.L. Pereira, C. Lutz, T. van Gerven, Experimental and numerical investigation of the effect of ultrasound on the growth kinetics of zeolite A, *Ultrason. Sonochem.* 82 (2022) 105909.
[34] S.G. Fegan, B.M. Lowe, Effect of alkalinity on the crystallisation of silicalite-1 precursors, *J. Chem. Soc., Faraday Trans. 1* 82 (3) (1986) 785.
[35] M.L. Guzman Castillo, F. Di Renzo, F. Fajula, J. Bousquet, Crystallization kinetics of zeolite omega, the synthetic analog of mazzite, *Microporous Mesoporous Mat.* 90 (1–3) (2006) 221–228.
[36] J. Bronić, A. Palčić, B. Subotić, L. Itani, V. Valtchev, Influence of alkalinity of the starting system on size and morphology of the zeolite A crystals, *Mater. Chem. Phys.* 132 (2–3) (2012) 973–976.
[37] D.D. Guo, B.J. Shen, Y.C. Qin, J.X. Sun, Q.X. Guo, S.Y. Ren, X.H. Gao, X.M. Pang, B. J. Wang, H.J. Zhao, H.H. Liu, USY zeolites with tunable mesoporosity designed by controlling framework Fe content and their catalytic cracking properties, *Microporous Mesoporous Mat.* 211 (2015) 192–199.
[38] F. Delprato, L. Delmotte, J.L. Guth, L. Huve, Synthesis of new silica-rich cubic and hexagonal faujasites using crown-etherbased supramolecules as templates, *Zeolites* 10 (6) (1990) 546–552.
[39] P. Lv, L.J. Yan, Y. Liu, M.J. Wang, W.R. Bao, F. Li, Catalytic conversion of coal pyrolysis vapors to light aromatics over hierarchical Y-type zeolites, *J. Energy Inst.* 93 (4) (2020) 1354–1363.
[40] B. Meng, S.Y. Ren, Z. Li, S.F. Nie, X.Y. Zhang, W.Y. Song, Q.X. Guo, B.J. Shen, A facile organic-free synthesis of high silica zeolite Y with small crystal in the presence of Co^{2+}, *Microporous Mesoporous Mat.* 323 (2021) 111248.